Electron-Doped Sr_2IrO_4: An Analogue of Hole-Doped Cuprate Superconductors Demonstrated by Scanning Tunneling Microscopy

Y. J. Yan,[1] M. Q. Ren,[1] H. C. Xu,[1] B. P. Xie,[1,2] R. Tao,[1] H. Y. Choi,[3] N. Lee,[3] Y. J. Choi,[3] T. Zhang,[1,2] and D. L. Feng[1,2,*]

[1]*State Key Laboratory of Surface Physics, Department of Physics, and Advanced Materials Laboratory, Fudan University, Shanghai 200433, China*

[2]*Collaborative Innovation Center of Advanced Microstructures, Fudan University, Shanghai 200433, China*

[3]*Department of Physics and IPAP, Yonsei University, Seoul 120-749, Korea*

(Received 17 June 2015; revised manuscript received 17 October 2015; published 4 November 2015)

Sr_2IrO_4 was predicted to be a high-temperature superconductor upon electron doping since it highly resembles the cuprates in crystal structure, electronic structure, and magnetic coupling constants. Here, we report a scanning tunneling microscopy/spectroscopy (STM/STS) study of Sr_2IrO_4 with surface electron doping by depositing potassium (K) atoms. We find that as the electron doping increases, the system gradually evolves from an insulating state to a normal metallic state, via a pseudogaplike phase, and a phase with a sharp, V-shaped low-energy gap with about 95% loss of density of state (DOS) at E_F. At certain K coverage (0.5–0.6 monolayer), the magnitude of the low-energy gap is 25–30 meV, and it closes at around 50 K. Our observations show that the electron-doped Sr_2IrO_4 remarkably resembles hole-doped cuprate superconductors.

DOI: 10.1103/PhysRevX.5.041018 Subject Areas: Superconductivity

The search for high-temperature superconductors (HTSC) has long been the pursuit of condensed-matter physics [1]. Recently, the $5d$ transition metal oxide Sr_2IrO_4 has attracted much attention because it possesses several distinct characteristics that are considered to be important for the high-temperature superconductivity [2–16]. Sr_2IrO_4 is isostructural to La_2CuO_4, which adopts the same quasi-two-dimensional (2D) layered perovskite structure of K_2NiF_4 [2–4]. The IrO_2 layers form a square lattice of Ir^{4+} ions with a nominal $5d^5$ configuration, and there is effectively one hole per Ir^{4+}. Because of the cooperation between spin-orbit coupling (SOC), crystal field, and Coulomb interaction with comparable strength, a pseudospin $j = 1/2$ (j being the total angular momentum) antiferromagnetic (AFM) Mott insulating state is realized in Sr_2IrO_4 at low temperature [5,6]. The low-energy magnetic excitations can be described by a $j = 1/2$ AFM Heisenberg model [5–11], and the nearest-neighbor AFM exchange interactions J are about 60–100 meV, which is comparable to that of cuprates [9,10]. The remarkable resemblance between Sr_2IrO_4 and cuprates makes Sr_2IrO_4 a good candidate for exploring unconventional HTSC upon carrier doping. Indeed, d-wave superconductivity by electron doping was predicted by several theoretical studies [11–13]. Meanwhile, a triplet p-wave pairing state in the hole-doped regime was also suggested when the Hund coupling was comparable to SOC [13]. Experimentally, electron doping was realized in Sr_2IrO_4 by La substitution, oxygen deficiency, or surface K dosing [4,14–16], while hole doping was realized by Rh substitution of Ir [17]. A unique electronic state with nodal quasiparticles and an antinodal pseudogap was found in the electron-underdoped regime by angle-resolved photoemission spectroscopy (ARPES) [14–16], resembling the underdoped cuprates. However, no experimental evidence of superconductivity has been found up to now. The search for superconductivity in doped Sr_2IrO_4 remains of great interest.

In this article, we report a low-temperature STM study on electron-doped Sr_2IrO_4 via *in situ* surface K dosing [14,18]. Sr_2IrO_4 single crystals were grown by a flux method using $SrCl_2$ flux. The sample was mounted onto the holder by conductive epoxy. After being precooled at 77 K in vacuum ($<1 \times 10^{-10}$ torr), the samples were cleaved and then immediately transferred into the STM head stabilized at 4.5 K. Stripelike Au contacts were evaporated onto the sample and the holder by a rasterlike mask to enhance tunneling channels. Thereafter, potassium atoms were evaporated onto the whole surface of the sample using commercial SAES alkali metal dispensers. Samples were kept at about 80 K during these operations. The surface coverage was precisely controlled by K flux and growth

*dlfeng@fudan.edu.cn

time. STM topography is taken in the constant current mode, and the dI/dV spectrum is collected using a standard lock-in technique with modulation frequency $f = 975$ Hz. A Pt tip was used for all the STM measurements after being treated on a Au (111) surface. The herringbone reconstruction and point defects on Au (111), together with the typical dI/dV spectrum of Au (111), can be routinely observed (see Fig. S1 in Ref. [19]).

Pristine Sr_2IrO_4 was cleaved in the vacuum at 77 K, leaving a charge-balanced SrO-terminated surface [20]. Figure 1(b) shows a 50×50 nm^2 topographic image measured at 77 K. The atomically resolved image with a square lattice is shown in the top inset. The Fourier transform (FT) of Fig. 1(b) (bottom inset) shows two sets of spots. Here, $\mathbf{q_1}$ is the Bragg spot of the SrO lattice, while $\mathbf{q_2}$ is from a $\sqrt{2}$ R45° reconstruction, which could be due to the rotation of the IrO_6 octahedra, as reported in Ref. [2]. Four types of defects are observed in the cleaved surface, as indicated by the arrows. The dI/dV spectrum measured at 77 K, away from defects, exhibits an insulating energy gap of about 700 meV, which is consistent with the previous STM report [20]. We found that the type-3 defects, which are likely oxygen defects [20], drastically suppress the insulating gap, as shown in Fig. 1(c). Other types of defects do not affect the local density of state (LDOS) significantly.

At temperatures lower than 30 K, we found that the tunneling cannot be obtained on pristine Sr_2IrO_4 because of drastically increased sample resistance (even upon surface K dosing). Thus, to introduce conducting channels, we evaporated Au contacts onto part of the cleaved surface through masks [Fig. 1(a) and Fig. S2 in Ref. [19]]. Then the tunneling to the region close to Au contacts is achieved at low temperatures. Figure 1(d) shows a topographic image of such a region (taken at 20 K); some scattered Au clusters can be seen on the surface. A slightly decreased insulating gap is observed in this region, indicating enhanced conductivity [Fig. 1(e), red curve]. This might be caused by some small amount of electrons transferred from the gold clusters to Sr_2IrO_4 (see Fig. S3 in Ref. [19] for details). Meanwhile, the insulating state is still maintained on Sr_2IrO_4 far away from the Au contacts. Thereafter, K atoms were evaporated on the surface to dope electron carriers [14,18], resulting in the final sample configuration sketched in Fig. 1(a). After depositing a certain amount of K (0.5–1 ML coverage), metallic state can be observed in the region close to the Au contacts [Fig. 1(e), blue curve] [21]. Figure 1(f) is a typical topographic image of such a region with 0.6 ML K coverage: the K atoms form clusters with a typical size of several nanometers. We then measured the tunneling spectrum in this region, as shown in Fig. 1(g). We found that for the K coverage of 0.5–0.7 ML, there is a sharp, V-shaped gap structure in the dI/dV spectrum, which is symmetric with respect to E_F. The gap magnitude changes with K coverage (25–30 meV for

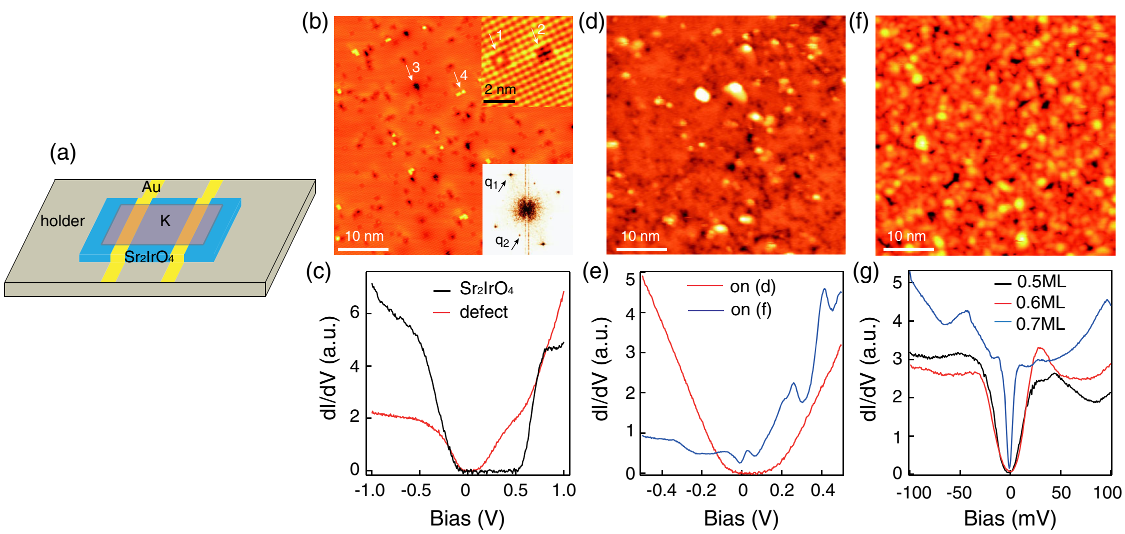

FIG. 1. Surface topography and dI/dV spectrum of Sr_2IrO_4 with and without K coverage. (a) Sketch of the sample configuration. (b) Typical topographic image on the SrO-terminated surface of pristine Sr_2IrO_4, measured at 77 K. The top and bottom insets represent the atomically resolved image and the FT of data in panel (b), respectively. Four different kinds of defects are indicated by arrows. (c) Spatially averaged dI/dV spectrum on the SrO-terminated surface. An insulating energy gap as large as 700 meV is observed on the defect-free region, while a reduced gap is observed on defects 3. (d) Typical topographic image of the SrO-terminated surface adjacent to Au contacts (measured at 20 K), in which a few Au clusters are observed as the white spots. (e) Spatially averaged dI/dV spectra measured on panels (d) and (f), showing a reduced insulating gap and a metallic state, respectively. (f) Typical topographic image after depositing 0.6 ML K atoms on the SrO-terminated surface that is adjacent to the Au contacts (measured at 20 K). (g) Representative dI/dV spectra on K-doped Sr_2IrO_4 with various K coverages (10 K for 0.5 ML, 20 K for 0.6 ML, 4.5 K for 0.7 ML), showing V-shaped gaps.

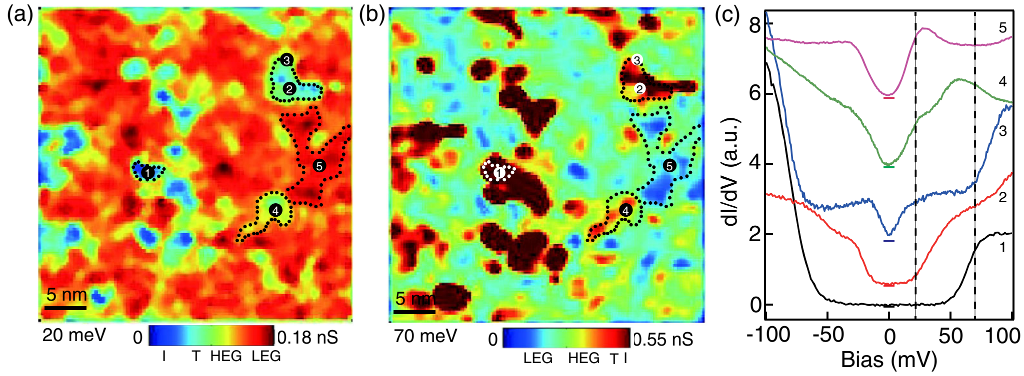

FIG. 2. Gap inhomogeneity of Sr_2IrO_4 with 0.6 ML K taken at 20 K. (a,b) dI/dV maps taken at $V_b = 20$ meV and 70 meV, respectively. Representative areas with different electronic states are marked by dotted lines. Each map has 100×100 pixels. (c) Typical dI/dV spectra taken at the positions marked by dots in panels (a) and (b), showing the evolution of electronic states across the regions. The horizontal bars indicate the zero conductance position of each curve. Dashed lines located at 20 meV and 70 meV are added as guides to the eye. The labels I, T, HEG, and LEG on the color bars indicate the insulating, transition, HEG-dominated, and LEG-dominated regions, respectively.

0.5 ML and 0.6 ML, 10 meV for 0.7 ML). Hereafter, it is called the low-energy gap or LEG, to distinguish it from the high-energy pseudogap previously found in ARPES [14–16]. For all the observed LEG's, about 95% of DOS vanishes near E_F.

To visualize the spatial distribution of this low-energy gap, we show the dI/dV map taken close to the gap edge at 20 meV in Fig. 2(a) (measured at 20 K), taking a sample with 0.6 ML-K dosing as an example (see also Fig. S4 in Ref. [19] for dI/dV maps at other energies). The spatial variation of tunneling conductance is reflected by the false color. There is a strong spatial inhomogeneity, or phase separation, between several types of patches, as highlighted by the color and representative dotted boundaries. The corresponding representative dI/dV spectra are shown in Fig. 2(c). With increasing conductance, there are generally four types of regions.

(1) The low-conductance region (the dark blue region) is the insulating region, which is characterized by an insulating gap larger than 100 meV in the corresponding spectrum [Fig. 2(c), curve 1].

(2) The transition region (the light blue and light green regions) is the region where the insulating gap is much smaller in the center of this region and gradually filled up at the boundary [Fig. 2(c), curves 2 and 3].

(3) The high-energy-gap (HEG) dominating region (the green and yellow regions) is the region where the LEG is present at 25–30 mV, but the dominating feature is a pseudogap-like feature at around the positive bias of 60 mV (defined as Δ_H), as shown by Fig. 2(c), curve 4.

(4) The LEG dominating region (the red region) is the region where a small symmetric V-shaped gap ubiquitously exists, as shown by curve 5 in Fig. 2(c). The gap is about 25–30 meV. This region is more homogeneous than others and is the majority one. The peaks at the gap edges are stronger here, while the HEG feature is weak or absent.

Similar electronic inhomogeneity has been observed in cuprates as well, which is attributed to inhomogeneous carrier distribution [22,23]. Since the K atoms were evaporated onto the sample surface holding at 80 K, which results in clustered surface morphology [Fig. 1(f)], the carrier concentration here is likely to have spatial inhomogeneity. As shown in Fig. 1(c), Sr_2IrO_4 is an insulator with an energy gap of about 700 meV. The observed lineshape evolution and transition between different regions clearly indicate that (1) the Mott gap of Sr_2IrO_4 is continuously suppressed by the increasing electron doping, and eventually disappears; (2) a HEG develops, which presumably is the antinodal pseudogap observed previously by ARPES [14]; and (3) with further electron doping, the phase with LEG gradually gains strength. In Fig. 2(b), we show the dI/dV map taken around the HEG energy at $V_b = 70$ mV. This map is clearly anticorrelated with the map taken at the LEG energy scale in Fig. 2(a), which may suggest the possible competition between these two states. All these behaviors share strong similarities with those of hole-doped cuprates, in which a Mott insulating state evolves into a pseudogap state and then a superconducting state with increasing hole doping [22,24].

The inhomogeneity of LDOS distribution is weakened with increasing K coverage (see Figs. S4 and S5 in Ref. [19]). However, the HEG and LEG features can be observed in a wide range of K coverage, as shown in Figs. 3(a) and 3(b). The energy scale of Δ_H decreases gradually with the increasing K coverage, as indicated by the arrows in Fig. 3(a). The distance between the two peaks at the gap edges of the typical dI/dV spectra defines $2\Delta_L$ (Δ_L is the gap magnitude of LEG). In Fig. 3(b), it is 54 meV for 0.5 ML and 59 meV for 0.6 ML, and it decreases to

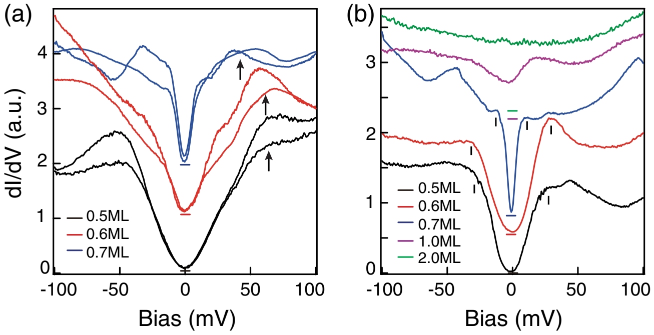

FIG. 3. K coverage dependence of dI/dV spectra. (a) The representative spectra taken at the HEG-dominated regions for various K coverages. Inhomogeneity of the pseudogap-like feature is illustrated by two spectra shown for each coverage. The arrows indicate the averaged energy locations of Δ_H. (b) The representative spectra taken at the LEG-dominated regions for 0.5–0.7 ML K coverage and arbitrary regions for 1–2 ML K coverage. The curves are offset vertically for clarity, and the horizontal markers indicate the zero conductance position of each curve. The data were taken at 10 K for 0.5 ML, 20 K for 0.6 ML, and 4.5 K for 0.7–2 ML.

22 meV for 0.7 ML. Considering the inhomogeneity of the gap magnitudes, the averaged Δ_L is about 28 meV for both 0.5 ML and 0.6 ML, and 10 meV for 0.7 ML, determined from the spatially averaged dI/dV spectra (see Fig. S7 in Ref. [19]). For Sr_2IrO_4 with 1 ML K coverage, the typical dI/dV spectrum (taken at 4.5 K) shows an overall flat DOS with only a small dip at E_F. As reported in Ref. [14] and observed in our ARPES results (see Fig. S8 in Ref. [19]), Sr_2IrO_4 with a 1-ML K overlayer shows quantum-well states with intense spectral weight, which indicates the formation of a metallic state in the K overlayer. Therefore, in this case, the LDOS will be contributed by both the metallic K overlayer and the underlying Sr_2IrO_4. Then, the small dip at E_F could be an indication of a possible gap in the K-dosed Sr_2IrO_4 layer. With further increasing K coverage, a normal metallic state is observed down to 4.5 K in the dI/dV spectrum without any indication of a gaplike structure, which possibly means that the system has entered the over-doped regime or that the states in the Sr_2IrO_4 layer are too weak to be detected. These doping behaviors also resemble those of the cuprates [22,24].

The temperature dependence of LEG is shown in Figs. 4(a)–4(c). For K coverage of 0.5–0.7 ML, the gap gradually fills up and the peaks at the gap edges are weakened as temperature increases. However, even after these peaks disappear [>60 K in Fig. 4(a)], there is still a broad V-shaped background, which may be induced by the HEG that could coexist with the LEG [22,25]. In the Supplemental Material [19] (Fig. S9), we show that such a growth of in-gap spectral weight is well beyond thermal broadening. To quantitatively study the temperature dependence of the LEG, we have defined gap depth = 1-ZBC/CP (ZBC: zero bias conductance,

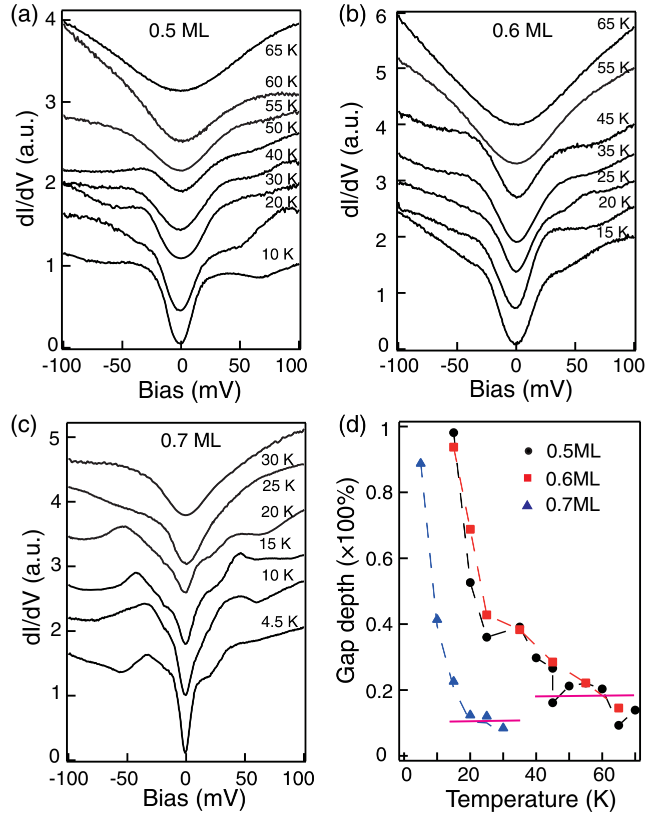

FIG. 4. Temperature dependence of the V-shaped gap. (a)–(c) Temperature dependence of the spatially averaged dI/dV spectra for K coverage of (a) 0.5 ML, (b) 0.6 ML, and (c) 0.7 ML, respectively. The spectra shown here are the average of the dI/dV spectra with large gap depth and visible peaks at the gap edges taken in the LEG-dominated regions of a 30×30 nm^2 area. The line-shape variations at different temperatures are caused by the lack of precisely tracking the same location on a clustered surface with strong LDOS inhomogeneity. The curves are offset vertically for clarity. (d) Gap depth (as defined in the main text) as a function of temperature, which decreases gradually with increasing temperature. T_L is defined by the temperature at which the gap depth stops decreasing quickly upon warming.

CP: averaged conductance of the two peaks at the gap edges), which is plotted in Fig. 4(d). The gap depth starts to increase rapidly upon cooling at 20 K for 0.7 ML, and at about 50 ± 5 K for both 0.5 ML and 0.6 ML. We assign these characteristic temperatures as the gap-closing temperatures for LEG (hereafter referred to as T_L).

In Fig. 5, we plot Δ_H, Δ_L, and T_L as a function of the K coverage. Δ_L and T_L scale with each other and appear to saturate at low K coverage, while Δ_H and the pseudogap measured by ARPES both increase with decreased coverage [14]. A detailed comparison between K-dosed Sr_2IrO_4 and a prototypical hole-doped cuprate is listed in Table I, demonstrating the remarkable analogy between these two systems. The doping evolution of the electronic states in electron-doped Sr_2IrO_4 found in our STM results is almost

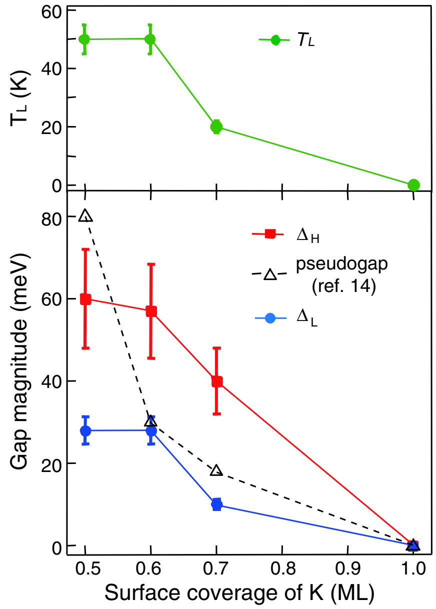

FIG. 5. Δ_H, Δ_L, and T_L as a function of the surface coverage of potassium. The gap magnitude of the pseudogap observed at the antinode by ARPES is shown by empty triangles for comparison [14].

the same as those found in a hole-doped cuprate. Theoretically, it has been shown that the low-energy electronic structure of Sr_2IrO_4 can be described by a 1/2-pseudospin Hubbard model, which is similar to the one that describes cuprates [11]. Moreover, because the sign of the next-nearest-neighbor hopping in Sr_2IrO_4 is opposite to that of the cuprate, the electron doping of Sr_2IrO_4 was suggested to be the analogue of hole doping of cuprates in early theoretical and experimental works [11,14]. Therefore, it naturally explains the similar doping dependence of both systems observed by ARPES and STM here [14,22,24,25]. Moreover, the energy scales of Sr_2IrO_4, such as the AFM exchange interactions and hopping integrals, were found to be about half of those of cuprates [9,10]. Intriguingly, the characteristic temperature scales and gap amplitude of the LEG are also about half of the optimally doped cuprates. These results all imply that, essentially, the similar Hamiltonians govern the physics of both systems. On the other hand, there are differences in these two systems. The strong spin-orbital coupling in the 5*d* electron systems makes the pseudospin instead of the spin the good quantum number to describe the magnetism. Moreover, the large coherence peak in superconducting cuprates is not clearly visible for the electron-doped Sr_2IrO_4, although some small sharp peaks do exist near E_F in the 0.7-ML K coverage case [Fig. 1(g)]. We speculate that this may be related to the fact that Sr_2IrO_4 seems to be more sensitive to impurities. It is also likely the reason why many other means of electron doping fail to make it conducting [4].

A remaining question is the origin of the LEG. We notice that in the literature, the gaplike feature around E_F may have various causes, such as density wave ordering, some "pseudogap" state, and superconductivity. For the first two cases, the gaps are usually not fully opened and they leave large residual DOS at E_F [22], as observed in most previous STM studies. In addition, no sign of charge density modulation is observed in our STM measurements (see FFTs of dI/dV maps in Fig. S6 in Ref. [19]) or in the previous photoemission measurements [14]. For a superconducting state, a fully gapped dI/dV spectrum with coherence peaks is usually observed, and a V-shaped gap appears in the presence of nodes. Therefore, the sharpness and nearly fully vanished DOS at E_F of the observed LEG make superconductivity a possible origin. This is actually the most important theoretical prediction made for the electron-doped Sr_2IrO_4 [11–13].

In summary, we have systematically studied the electronic states of Sr_2IrO_4 with different surface K coverage. At the K coverage of 0.5–0.7 ML, we observed a sharp,

TABLE I. Comparison of K-dosed Sr_2IrO_4 and hole-doped cuprates.

	K-doped Sr_2IrO_4	Hole-doped cuprate (Bi2212)
Electronic states with increased carrier concentrations	Mott insulator Pseudogap-like HEG-dominated state V-shaped LEG-dominated state Normal metallic state	Mott insulator Pseudogap state Superconductivity with V-shaped d-wave gap Normal metallic state
Magnetism	Pseudospin $j = 1/2$ Nearest-neighbor AFM exchange interaction $J \sim 0.06 - 0.1$ eV	Spin $s = 1/2$ Nearest-neighbor AFM exchange interaction $J \sim 0.12$ eV
Low-energy gap	V-shaped, d-wave? 25–30 meV at maximum	V-shaped, d-wave About 35 meV at optimal doping
Characteristic temperature of LEG	$T_L \sim 50 \pm 5$ K	$T_c \sim 90$ K

V-shaped gap with nearly vanished DOS at E_F. We also demonstrated that with increased surface K coverage, the electronic state of Sr_2IrO_4 evolves from an insulating state to a normal metallic state with more than 1 ML K, via a pseudogap-like state and a V-shape-gapped state, sequentially. The remarkable analogy between this system and hole-doped cuprates, particularly the low-energy gap feature, the characteristic temperature, and the evolution of various electronic states with doping, is consistent with the previous theoretical prediction of the possible superconductivity in Sr_2IrO_4. Efforts are in progress to look for further evidence of superconductivity, such as magnetic vortex, zero resistance, and the Meissner effect.

ACKNOWLEDGMENTS

We thank Professor Changyoung Kim for helping set up the collaboration, and Professor Fa Wang for helpful discussions. This work is supported by the National Science Foundation of China, and National Basic Research Program of China (973 Program) under Grant No. 2012CB921402. The work at Yonsei was supported by the NRF Grants No. NRF-2013R1A1A2058155 and No. NRF-2014S1A2A2028481, and partially by the Yonsei University Future-Leading Research Initiative of 2014 (2014-22-0123).

Note added.—Recently, we become aware of another independent ARPES work by Y. K. Kim *et al.* (arXiv: 1506.06639) on a similar system, which reports the observation of a *d*-wave gap that is of similar magnitude to the possible superconducting gap found here. Thus, it is consistent with our work.

[1] J. G. Bednorz, and K. A. Müller, *Possible High-Tc Superconductivity in the Ba-La-Cu-O System*, Z. Phys. B **64**, 189 (1986).

[2] M. K. Crawford, M. A. Subramanian, R. L. Harlow, J. A. Fernandez-Baca, Z. R. Wang, and D. C. Johnston, *Structural and Magnetic Studies of* Sr_2IrO_4, Phys. Rev. B **49**, 9198 (1994); Sr_2RhO_4 *and* Sr_2IrO_4*: Structural and Magnetic Studies of 4d and 5d Transition Metal Analogs of* La_2CuO_4, Physica (Amsterdam) **235C**, 743 (1994).

[3] G. Cao, J. Bolivar, S. McCall, J. E. Crow, and R. P. Guertin, *Weak Ferromagnetism, Metal-to-Nonmetal Transition, and Negative Differential Resistivity in Single-Crystal* Sr_2IrO_4, Phys. Rev. B **57**, R11039 (1998).

[4] O. B. Korneta, T. Qi, S. Chikara, S. Parkin, L. E. De Long, P. Schlottmann, and G. Cao, *Electron-Doped* $Sr_2IrO_{4-\delta}$ *(*$0 \le \delta \le 0.04$*): Evolution of a Disordered* $J_{eff} = 12$ *Mott Insulator into an Exotic Metallic State*, Phys. Rev. B **82**, 115117 (2010).

[5] B. J. Kim *et al.*, *Novel* $J_{eff} = 1/2$ *Mott State Induced by Relativistic Spin-Orbit Coupling in* Sr_2IrO_4, Phys. Rev. Lett. **101**, 076402 (2008).

[6] B. J. Kim, H. Ohsumi, T. Komesu, S. Sakai, T. Morita, H. Takagi, and T. Arima, *Phase-Sensitive Observation of a Spin-Orbital Mott State in* Sr_2IrO_4, Science **323**, 1329 (2009).

[7] H. Jin, H. Jeong, T. Ozaki, and J. Yu, *Anisotropic Exchange Interactions of Spin-Orbit-Integrated States in* Sr_2IrO_4, Phys. Rev. B **80**, 075112 (2009).

[8] S. J. Moon *et al.*, *Dimensionality-Controlled Insulator-Metal Transition and Correlated Metallic State in 5d Transition Metal Oxides* $Sr_{n+1}Ir_nO_{3n+1}$ *(*n = 1*, 2, and* ∞*)*, Phys. Rev. Lett. **101**, 226402 (2008).

[9] J. Kim *et al.*, *Magnetic Excitation Spectra of* Sr_2IrO_4 *Probed by Resonant Inelastic X-Ray Scattering: Establishing Links to Cuprate Superconductors*, Phys. Rev. Lett. **108**, 177003 (2012).

[10] S. Fujiyama, H. Ohsumi, T. Komesu, J. Matsuno, B. J. Kim, M. Takata, T. Arima, and H. Takagi, *Two-Dimensional Heisenberg Behavior of* $J_{eff} = 1/2$ *Isospins in the Paramagnetic State of the Spin-Orbital Mott Insulator* Sr_2IrO_4, Phys. Rev. Lett. **108**, 247212 (2012).

[11] F. Wang, and T. Senthil, *Twisted Hubbard Model for* Sr_2IrO_4*: Magnetism and Possible High Temperature Superconductivity*, Phys. Rev. Lett. **106**, 136402 (2011).

[12] H. Watanabe, T. Shirakawa, and S. Yunoki, *Monte Carlo Study of an Unconventional Superconducting Phase in Iridium Oxide* $J_{eff} = 1/2$ *Mott Insulators Induced by Carrier Doping*, Phys. Rev. Lett. **110**, 027002 (2013).

[13] Z. Y. Meng, Y. B. Kim, and H.-Y. Kee, *Odd-Parity Triplet Superconducting Phase in Multiorbital Materials with a Strong Spin-Orbit Coupling: Application to Doped* Sr_2IrO_4, Phys. Rev. Lett. **113**, 177003 (2014).

[14] Y. K. Kim, O. Krupin, J. D. Denlinger, A. Bostwick, E. Rotenberg, Q. Zhao, J. F. Mitchell, J. W. Allen, and B. J. Kim, *Fermi Arcs in a Doped Pseudospin-*1/2 *Heisenberg Antiferromagnet*, Science **345**, 187 (2014).

[15] M.-Y. Li, Z.-T. Liu, H.-F. Yang, J.-L. Zhao, Q. Yao, C.-C. Fan, J.-S. Liu, B. Gao, D.-W. Shen, and X.-M. Xie, *Tuning the Electronic Structure of* Sr_2IrO_4 *Thin Films by Bulk Electronic Doping Using Molecular Beam Epitaxy*, Chin. Phys. Lett. **32**, 057402 (2015).

[16] A. de la Torre *et al.*, *Collapse of the Mott Gap and Emergence of a Nodal Liquid in Lightly Doped* Sr_2IrO_4, Phys. Rev. Lett. **115**, 176402 (2015).

[17] J. P. Clancy, A. Lupascu, H. Gretarsson, Z. Islam, Y. F. Hu, D. Casa, C. S. Nelson, S. C. LaMarra, G. Cao, and Y.-J. Kim, *Dilute Magnetism and Spin-Orbital Percolation Effects in* $Sr_2Ir_{1-x}Rh_xO_4$, Phys. Rev. B **89**, 054409 (2014).

[18] D. Fournier *et al.*, *Loss of Nodal Quasiparticle Integrity in Underdoped* $YBa_2Cu_3O_{6+x}$, Nat. Phys. **6**, 905 (2010).

[19] See Supplemental Material at http://link.aps.org/supplemental/10.1103/PhysRevX.5.041018 for Figs. S1 to S9.

[20] J. Dai, E. Calleja, G. Cao, and K. McElroy, *Local Density of States Study of a Spin-Orbit-Coupling Induced Mott Insulator* Sr_2IrO_4, Phys. Rev. B **90**, 041102(R) (2014).

[21] The regions far away from the Au contacts can be metallic as well, but they cannot be observed by STM at low temperatures because of the lack of percolation conducting path likely caused by isolated conductive patches.

[22] Ø. Fischer, M. Kugler, I. Maggio-Aprile, C. Berthod, and C. Renner *Scanning Tunneling Spectroscopy of*

High-Temperature Superconductors, Rev. Mod. Phys. **79**, 353 (2007).

[23] K. McElroy, D.-H. Lee, J. E. Hoffman, K. M. Lang, J. Lee, E. W. Hudson, H. Eisaki, S. Uchida, and J. C. Davis, *Coincidence of Checkerboard Charge Order and Antinodal State Decoherence in Strongly Underdoped Superconducting* $Bi_2Sr_2CaCu_2O_{8+\delta}$, Phys. Rev. Lett. **94**, 197005 (2005).

[24] A. Damascelli, Z. Hussain, and Z.-X. Shen, *Angle-Resolved Photoemission Studies of the Cuprate Superconductors*, Rev. Mod. Phys. **75**, 473 (2003).

[25] Ch. Renner, B. Revaz, J.-Y. Genoud, K. Kadowaki, and Ø. Fischer, *Pseudogap Precursor of the Superconducting Gap in Under- and Overdoped* $Bi_2Sr_2CaCu_2O_{8+\delta}$, Phys. Rev. Lett. **80**, 149 (1998).